EXPERIMENTS WITH ATMOSPHERIC PRIMITIVE-EQUATION MODELS

by

Philip Garland Kesel

UNITED STATES
NAVAL POSTGRADUATE SCHOOL

THESIS

EXPERIMENTS WITH ATMOSPHERIC PRIMITIVE-EQUATION MODELS

by

Philip Garland Kesel

December 1968

[redacted]

EXPERIMENTS WITH ATMOSPHERIC PRIMITIVE EQUATION MODELS

by

Philip Garland Kesel
Lieutenant, United States Navy
B.S., University of Utah, 1962

Submitted in partial fulfillment of the
requirements for the degree of

MASTER OF SCIENCE IN METEOROLOGY

from the

NAVAL POSTGRADUATE SCHOOL
December 1968

ABSTRACT

Two atmospheric prediction models, based upon the meteorological primitive equations, were programmed and tested on the CDC 6500 computer. A frictionless, barotropic model was integrated, using ten-minute time steps, at 500 MBS for periods up to four days. Then, an n-level, baroclinic model for an inviscid, adiabatic atmosphere was integrated for brief test periods at five uniformly-spaced zeta (sigma) surfaces over a smooth earth. Both models were initialized with actual data fields provided by FNWC Monterey.

Acceptability was based on measurements of energy and vorticity parameters, as well as on qualitative assessments of output fields. The barotropic 500 MB height forecasts were found to be comparable to the FNWC (vorticity model) barotropic forecasts. Mean-square-vorticity and kinetic energy were suitably conserved for integrations up to four days. An energy accumulation in the smaller range of scale was increasingly evident beyond two days into the forecast period. No smoothing was performed to control this accumulation. A limited number of test integrations was made with the five-level model. Computational instabilities were observed for forecasts beyond twelve hours. Interim results are presented.

TABLE OF CONTENTS

EXPERIMENTS WITH ATMOSPHERIC PRIMITIVE-EQUATION MODELS

by

Philip Garland Kesel

ERRATA SHEET

Page 9	Line 3 should read: Naval Postgraduate School, Monterey, California
Page 13	Paragraph 1, line 5: read "boundary-condition" vice "boundary condition"
Page 15	Paragraph 1, line 2: read "short-range" vice "short range"
Page 20	Paragraph 2, line 1: read "this research" vice "thesis research"
Page 25	Line 1: read "small-scale" vice "small scale"
Page 30	Line 5: read "height-error" vice "height error"
Page 43	Line 14: read "Haltiner (4)" vice "Haltiner (3)"
Page 45	Section 3.5, line 4: read "tape;" vice "tape:"
Page 49	Paragraph 5, line 1: read "series of test runs is"
Page 58	Paragraph 2, line 1: read "see Haltiner (4), for example"
	Paragraph 3, line 2: read "pressure-force" vice "pressure force"

LIST OF CHARTS

LIST OF FIGURES

TABLE OF SYMBOLS AND ABBREVIATIONS

CDC	Control Data Corporation
FNWC	Fleet Numerical Weather Central, Monterey
NPGS	Navy Postgraduate School, Monterey
MB	millibar(s)
f	Coriolis parameter
$\bar{f}$	value of f at 45° latitude
h	height of free surface (barotropic experiment)
$\mathbb{V}$	wind velocity
σ	vertical coordinate in Phillip's (sigma) system, which specifies a pressure (surface) as some fraction of the pressure at the lower boundary
ζ	vertical coordinate in NPGS (zeta) coordinate system, wherein zeta is an arbitrary function of sigma
$\hat{\zeta}$	relative vorticity
$\hat{\delta}$	velocity divergence
g	upward component of the apparent gravitational acceleration
m	horizontal map factor
s	vertical map factor (which arises from sigma-to-zeta transformation)
d	horizontal mesh length (381 kilometers at 60° latitude)
Φ	the geopotential
Ψ	stream function for the non-divergent wind component
$\dot{\sigma}$	vertical velocity in the sigma system
w	vertical velocity in the zeta system ($w = -\dot{\sigma}$)
p	atmospheric pressure
π	pressure at lower boundary
R	gas constant
∇	del operator

∇	finite-difference del operator
∇^2	Laplacian operator
∇^2	finite-difference Laplacian operator
J	Jacobian operator
Δ	incremental change
c_p	specific heat at constant pressure
X	abscissa of stereographic rectangular coordinate
Y	ordinate of stereographic rectangular coordinate
t	time
u	zonal wind component relative to the grid array
v	meridional wind component relative to the grid array
T	absolute temperature
a	mean earth radius
Ω	angular velocity of the earth
E_p	total potential energy (internal plus geopotential)
E_k	total kinetic energy
SVP	a parameter proportional to the square of the relative vorticity (summed over all grid points)

ACKNOWLEDGEMENTS

The author is indebted to Professor G.J. Haltiner, both for stimulating discussions and counsel during the course of this investigation.

In addition to making several beneficial suggestions, Professor R.T. Williams also provided the conservation forms (and proof) of the finite-difference scheme used in the baroclinic experiment.

The computer support, provided by Captain P.M. Wolff, USN, was greatly appreciated. The author would also like to express his thanks to several members of Captain Wolff's staff, particularly LCDR H. Nicholson, USN, and Mr. Leo Clarke, who provided coordination of computer services and hemispheric data fields, respectively.

1.0 INTRODUCTION

Disadvantages arising from more generalized forms of the vorticity, divergence, and thermodynamic equations have overshadowed the advantage of relatively large integration time steps in filtered prediction models. At the same time, increased knowledge in finite-difference techniques, in initialization procedures, and in boundary condition formulation, have been realized in a decade marked by unbelievable increases in computer capacity and speeds. These trends and accomplishments have accelerated the shift to the so-called "primitive equations" as a basis for atmospheric prediction models, both operational and research.

1.1 Finite Differencing

Whereas, in filtered models, an integration time step of one hour is possible without risk of linear computational instability, the corresponding time step for primitive-equation integrations is approximately ten minutes. One must fulfill the von Neumann stability criterion in order to avoid this type of instability in linear differential equations. A second type of instability may arise in spite of careful selection of time step and grid mesh length. This is the non-linear computational instability, or "aliasing", first described by Phillips (1959). Although Phillips treated non-linear differential equations, Miyakoda (1962) showed that non-linear instability can also occur in special types of linear equations.

Aliasing is described by Lilly (1965) for regions in which some arbitrary continuous function is being represented by a finite number of gridded values. It is shown that there exists a maximum and minimum wavelength which can be resolved by any grid array, and that waves outside of this range will be misrepresented in terms of the permitted harmonics.

Phillips controlled this phenomenon by smoothing. It may be reduced significantly, however, by use of conservation forms of the difference analogs, especially those which preserve the average wave number. The latter prevent the cascade of energy toward smaller ranges of scale. The well-known methods of Arakawa (1966) represent those which conserve mean-square vorticity, total kinetic energy, and average wave number. Phase errors are not eliminated by conservation forms, but their magnitudes are tolerable.

Another potential difficulty is associated with the phrasing of time derivatives, which have taken on a new significance with the advances made in space-differencing methods. The work of Kurihara (1965), Lilly (1965), and Young (1968), is illustrative of efforts to study, and possibly, to reduce the "slow" instability associated with the various time-differencing schemes. The "leapfrog" scheme of Richtmyer (1963) has been used widely in spite of its shortcomings. These may be listed as follows:

a. kinetic energy is not conserved.

b. during extended integrations, non-linear instability may develop in the absence of some form of smoothing.

c. the odd- and even-solution sets tend to proceed independently of each other because of the alternating sign of the computational mode. (some form of solution averaging may be helpful to eliminate the latter difficulty). In spite of these shortcomings, the leapfrog scheme is used because of the implied economies and its general accuracy.

The finite-differencing scheme ultimately selected for a given model is one which best compromises its associated: (1) diffusive characteristics; (2) existence and properties of any computational mode; (3) stability properties; and (4), the computational burden.

1.2 Boundary Conditions

The boundary conditions for any model must be tailored both to the specific equation set and to the objective of the integrations (short range forecast, or long-term general circulation experiment). The primitive-equation free-surface barotropic forecast model of Shuman and Vanderman (1966) is indicative of the effects of approximate versus correct boundary conditions on the forecast fields. Shuman showed that the RMS velocity divergence was tolerably conserved for periods up to about thirteen days when using approximate boundary conditions, but that the model "blew up" rapidly therafter. By using the correct boundary conditions (which were consistent with the equations), the model not only conserved RMS velocity divergence from the outset, but also prevented further deterioration of the forecast which used the approximate conditions for the first thirteen days.

The important point is that incorrect boundary conditions (as well as discretization errors) may excite gravity-inertial waves which, in the absence of some dissipative mechanism, may contaminate the forecast. See Nitta and Hovermale (1967) for an interesting discussion of these matters. Matsuno (1966) reported on false reflections of the computational mode from an outflow boundary. This inward propagation of errors was especially prominent at the shorter wavelengths. The rate of reflection decreased with increasing wavelength and with increasing "order" of continuity at the lateral boundaries. Thus, to overcome this effect, an increasing number of interior points is required to approximate the boundary value of an advected parameter (if a suitable assumption or approximation cannot be found for the particular problem).

1.3 Initialization Procedures

Initialization procedures are probably the least well-known of the requirements for model development. The whole problem of weather analysis and forecasting is concerned with the mutual adjustment between the mass and motion fields under the influence of rotation and gravity.

One very interesting result arose from the general circulation experiments of Smagorinsky (1965). Patterns of precipitation appeared roughly the same regardless of the initial condition of vertical motion, provided that other initial conditions (such as temperature and the non-divergent wind component) are held fixed. Miyakoda and Moyer (1968) suggest that for periods of more than five days (for the integrations), the vertical motion initialization is somewhat arbitrary because of the deterministic nature of the equations.

Initialization falls into two classes: (1) extrapolative, and (2) iterative. In either case, the idea is to reduce the noise and to represent only the slowly changing meteorological state. The former type consists of a marching integration of the equations to arrive at this "balanced" condition. The latter type stays at the same time level, but iterates the computations until the equilibrium state is reached. Clearly, the choice depends upon the model purpose. The iterative method would have an advantage for users requiring accurate short-term forecasts (of the order of a few hours, say), whereas the extrapolative method would be entirely satisfactory for forecast periods beyond the time required to "settle down" (ten hours or longer, say).

Thus far, primitive-equation models have been used with an assortment of initial fields - some real and some analytical constructions. Linearized research models may be initialized according to some preselected analytical distribution with a known solution.

In contrast, Shuman and Hovermale (1967) chose to use as initial data the objective analyses of geopotential height and temperature at the ten mandatory pressure levels (from 1000 to 100 MBS). Each of the input analyses was expanded from the JNWP octagonal grid into a 53 x 57 rectangular array by an extrapolative scheme which consisted of: (1) finding the mean value of the analyzed quantity on the octagon boundary, and copying this value into the non-overlapping portion (border region) of the 53 x 57 array; and (2) "wedding" the two regions by means of a "ring" smoother, while holding the boundary of the rectangular array fixed. By this process, one recognizes that the equatorial regions would be virtually devoid of small scale components.

The removal, or reduction, of these small-scale features is clearly justified for several reasons, not the least of which is the general inappropriateness of the so-called balance equation in the tropics. The difficulties, moreover, of false reflections as reported by Matsuno (1966) would be minimized in such "flat" fields. By flattening a field in this way, one clearly "increases the order of continuity" at the expense of accurate specification of meteorological detail in the tropics in order to preclude possible computational difficulties.

The finite-difference schemes, boundary conditions, and initialization procedures for the models studied in this paper will be discussed in detail in the appropriate sections of this thesis.

1.4 Coordinate Systems

Historically, the (x,y,p,t) coordinate system was shown to be superior to the rectangular system in many respects, but it suffered from the difficulties arising from the lower boundary condition.

Over smooth terrain, one generally assumes that the vertical velocity vanishes identically at the lower boundary; whereas, over rough terrain, one assumes that

$$\omega \doteq \mathbb{V} \cdot \nabla \pi$$

(or some equivalent approximation) where π is the terrain pressure.

In Phillip's (x, y, σ, t) sigma system, the particular problem just mentioned is overcome, but the sigma system is not entirely free of practical difficulties. Kurihara (1968) reported, for example, on problems arising from (large) terrain-pressure gradients.

In this research project, the barotropic model was written in pressure coordinates, but the baroclinic model was based upon a generalized "zeta" system which was proposed by R.T. Williams (personal communication). In this modified sigma system, the vertical coordinate zeta is related to Phillip's sigma by an arbitrary functional relationship

$$\sigma = f(\zeta)$$

where, it is clear, one may achieve the desired "linearity" in the vertical parameter while allowing for arbitrary placement of the computational surfaces.

2.0 THE BAROTROPIC EXPERIMENT

2.1 Introduction

The matter of testing a simple barotropic model prior to engaging in more complex simulations is a desirable approach. The work of Houghton et al (1966) and Shuman and Vanderman (1966) is cited in this regard.

Houghton conducted experiments with various finite-difference formulations for the Coriolis term and boundary conditions in order to observe sensitivities in long-term solutions. Solution stability was achieved without a large amount of smoothing, but some was necessary in order to control truncation errors. Charney (1965) had suggested an upper limit (several weeks) for long-term integrations because of inaccuracies in initial conditions. Houghton allowed that stability and truncation effects may be of equal importance to the validity of long-term solutions as to the growth of initial error.

In this project, the author has speculated that the small errors, or inconsistencies, in the initial conditions, as well as the effects of truncation and discretication, will not be of major concern for short-term integrations. There does appear to be some basis for more concern about the former in one- and two-day forecasts.

Shuman and Vanderman (1966) also tested a primitive-equation free-surface barotropic model in a tropical channel experiment. They concluded that approximate boundary conditions (which were inconsistent with the difference analogs) were entirely satisfactory for integrations up to about twelve days. The philosophy behind Shuman's choice was that the conditions provided for reflection of pure gravity waves at the walls. The inertial effects (due to the presence of "f"), it was reasoned, could be ignored for a limited time.

The finite-difference analog referred to by Shuman as the "semi-momentum" form apparently contains a large amount of smoothing because of the generous use of the superbars. This may account not only for the success of the long-term integrations without explicit smoothing, but also for the degree of concern about "unsmoothing" before use of the balance equation.

2.2 Purpose of the Barotropic Experiment

The first phase of thesis research consisted of the derivation, programming (CDC 6500), and evaluation of a barotropic free-surface model. This was test run at the 500 MB level using, as initial data, the actual objectively-analyzed hemispheric data fields provided by FNWC Monterey.

The author, after noting the many achievements of investigators cited earlier, felt that the obstacles remaining for reasonably-accurate short-term integrations of real data fields were more practical than theoretical. If would instructive, that is, to see if approximations and assumptions found suitable in analytical test integrations were equally suitable for integrations with real data fields.

The purpose of the barotropic experiment was to note the suitability of certain boundary conditions, to determine appropriate initialization procedures, and to test the modified-Arakawa finite-difference analogs (as proposed by R.T. Williams) for a model which might be expected to reasonably simulate atmospheric flow patterns at 500 MBS for periods up to four days.

2.3 The System of Prognostic Equations

The two-dimensional differential equations of momentum and continuity for a free-surface barotropic, inviscid atmosphere may be approximated on a polar stereographic projection as follows:

a. momentum equation in east-west direction:

$$\frac{\partial uh}{\partial t} = h\left\{vf - mg\frac{\partial h}{\partial x} - u\left(u\frac{\partial m}{\partial x} + v\frac{\partial m}{\partial y}\right)\right\} - m^2\left\{\frac{\partial}{\partial x}\left(\frac{hu^2}{m}\right) + \frac{\partial}{\partial y}\left(\frac{huv}{m}\right)\right\} \qquad (2.3.1)$$

b. momentum equation in north-south direction:

$$\frac{\partial vh}{\partial t} = -h\left\{uf + mg\frac{\partial h}{\partial y} + v\left(u\frac{\partial m}{\partial x} + v\frac{\partial m}{\partial y}\right)\right\} - m^2\left\{\frac{\partial}{\partial x}\left(\frac{huv}{m}\right) + \frac{\partial}{\partial y}\left(\frac{hv^2}{m}\right)\right\} \qquad (2.3.2)$$

c. continuity equation:

$$\frac{\partial h}{\partial t} = -m\left\{\frac{\partial}{\partial x}(uh) + \frac{\partial}{\partial y}(vh)\right\} \qquad (2.3.3)$$

The reader is referred to Appendix A for the development of this set of equations in flux form.

The computational boundary was taken to be mid-way between the outer ring of grid points and the first interior ring of points. This permitted the practical application of boundary conditions required for conserving the square of any parameter being advected, while at the same time, permitting non-zero normal wind components at the first interior ring.

Geostrophic flow was assumed for the normal wind component along the first interior ring of points because of the computational convenience. By so doing, the problem of computing the correct values of "h" along the outermost ring is avoided.

The advective terms led to the following boundary conditions. At the computational boundaries parallel to the y-axis,

$$\overline{\left(\frac{uh}{m}\right)}^{x} = 0 \qquad (2.3.4)$$

while, at the boundaries parallel to the x-axis,

$$\overline{\left(\frac{vh}{m}\right)}^{y} = 0 \qquad (2.3.5)$$

For convenience, the tangential wind component at the first interior ring was copied into the adjacent grid points on the outermost ring. In a similar manner, the values of "h" were also shifted "out" for convenience.

It will be seen that since the minimum value of the Coriolis parameter permitted was that value corresponding to "f" at 15^{o} latitude, the map factor advection terms (which are small anyway) vanish south of that latitude. The local change of "uh" and "vh" depended, therefore, on the horizontal flux divergence terms at the first interior ring (since geostrophic flow was assumed). Single (space) differences were used as appropriate in the continuity equation along the first interior ring.

Initialization of wind components consisted of solving the so-called linear balance equation of the form

$$\nabla^2 \Phi = \nabla \cdot (f \nabla \psi) \qquad (2.3.6)$$

using an FNWC 500 MB height field. The "first guess" streamfunction values were taken to be

$$\psi^o = \frac{g h^o}{f} \qquad (2.3.7)$$

where h^o was the initial height value at each point.

The integration time step was ten minutes. Subsequent to an initial forward (single) step, a conventional centered difference was used.

2.4 Finite Difference Forms

A modified-Arakawa finite-difference scheme was employed. In this scheme, the momentum and continuity equation analogs were expressed in the forms shown below:

a. momentum equation in east-west direction:

$$(uh)_{i,j}^{n+1} = (uh)_{i,j}^{n-1} + 2\Delta t \left\{ -\mathcal{L}(u)_{i,j} + h_{i,j} \left[(fv)_{i,j} - g \frac{m_{i,j}}{2d} (h_{i+1,j} - h_{i-1,j}) - \frac{u_{i,j}}{2d} \left\{ u_{i,j} (m_{i+1,j} - m_{i-1,j}) + v_{i,j} (m_{i,j+1} - m_{i,j-1}) \right\} \right] \right\}^n \qquad (2.4.1)$$

b. momentum equation in north-south direction:

$$(vh)_{i,j}^{m+1} = (vh)_{i,j}^{m-1} + 2\Delta t\left\{-\mathcal{L}(v)_{i,j} - h_{i,j}\left[(fu)_{i,j}\right.\right.$$

$$+ \frac{g}{2d} m_{i,j}(h_{i,j+1} - h_{i,j-1}) + \frac{v_{i,j}}{2d}\left\{u_{i,j}(m_{i+1,j} - m_{i-1,j})\right.$$

$$\left.\left.\left. + v_{i,j}(m_{i,j+1} - m_{i,j-1})\right\}\right]\right\}^{n} \qquad (2.4.2)$$

where, for any advected parameter, ψ, we have defined the operator

$$\mathcal{L}(\psi)_{i,j} = \frac{m^2_{i,j}}{4d}\left[\left\{\left(\frac{uh}{m}\right)_{i+1,j} + \left(\frac{uh}{m}\right)_{i,j}\right\}\cdot\left\{\psi_{i+1,j} + \psi_{i,j}\right\}\right.$$

$$- \left\{\left(\frac{uh}{m}\right)_{i-1,j} + \left(\frac{uh}{m}\right)_{i,j}\right\}\cdot\left\{\psi_{i-1,j} + \psi_{i,j}\right\}$$

$$+ \left\{\left(\frac{vh}{m}\right)_{i,j+1} + \left(\frac{vh}{m}\right)_{i,j}\right\}\cdot\left\{\psi_{i,j+1} + \psi_{i,j}\right\}$$

$$\left. - \left\{\left(\frac{vh}{m}\right)_{i,j-1} + \left(\frac{vh}{m}\right)_{i,j}\right\}\cdot\left\{\psi_{i,j-1} + \psi_{i,j}\right\}\right] \qquad (2.4.3)$$

c. continuity equation:

$$h_{i,j}^{m+1} = h_{i,j}^{n-1} + 2\Delta t\left\{-\frac{m_{i,j}}{2d}\left[(uh)_{i+1,j}\right.\right.$$

$$\left.\left. - (uh)_{i-1,j} + (vh)_{i,j+1} - (vh)_{i,j-1}\right]\right\}^{n} \qquad (2.4.4)$$

where "n" denotes the time level.

In an attempt to reduce some of the small scale irregularities of the initial height analyses near the computational boundary, a five-point smoother routine was written to produce the following effect. First,a mean height value (say) was calculated for the outermost grid ring. This value was set at all of the outermost ring points. The smoothing coefficient was latitude dependent in the sense that the smoothing increased from zero at 20^{o} latitude to a degree sufficient to remove all perturbations at the outermost ring. This procedure was deemed to be consistent with, and justified by, the linear balance assumption in the tropics.

2.5 Research Procedures and Results

The barotropic model was tested on actual FNWC 500 MB height analyses for the Northern Hemisphere, rather than on some idealized distribution for which some analytical solution was known. This less rigorous test was consistent with the purpose of the study - to see if some of the approximations found suitable for analytical tests were equally suitable for use with actual data fields (and their much larger frequency ranges).

The judgement as to solution stability or acceptability was based on certain diagnostic parameters, such as the square-vorticity parameter (SVP) or mean kinetic energy (KE), as well as on the meteorological appearance of the output fields.

The first test consisted of computing all parameters and terms as they appeared in the equations (without space averaging). Then, the model was rerun using space averaging in a manner similar to that used by Shuman (1966). It was determined that the SVP grew at an intolerably large rate.

When no space averaging was performed, the SVP growth rate was an order of magnitude smaller. In spite of the lesser rate, however, energy did tend to accumulate in the smaller range of scale, particularly in tropical regions.

A second test consisted of measuring the SVP for a run in which the integration cycle was restarted every 72 time steps, but with no space averaging. This was an attempt to measure the effects of non-linear interactions between the odd- and even-solution sets. The result was that the SVP grew at approximately the same rate for both runs, but the SVP took a small step upward in value immediately following the restart.

Figure 1 depicts the aforementioned SVP growth rates. The upper curve (A) shows the rate for the case when space averaging was used, but no restarting was performed. The lower curve (B) shows the SVP rate for both cases in which no space averaging was performed (no attempt was made to indicate the small upward jogs after each restart, since they were negligible on this scale). The larger rate (A) was judged to be the result of some rather serious imbalances caused by not "unsmoothing" initial fields in the manner reported by Shuman (1966, 1967). The much smaller rate (B) was most likely caused by small imbalances arising from the use of the linear balance equation, and by the gradual accumulation (which could be either a real or computationally-induced cascade) of energy in the small scale features. No smoothing was performed in case B.

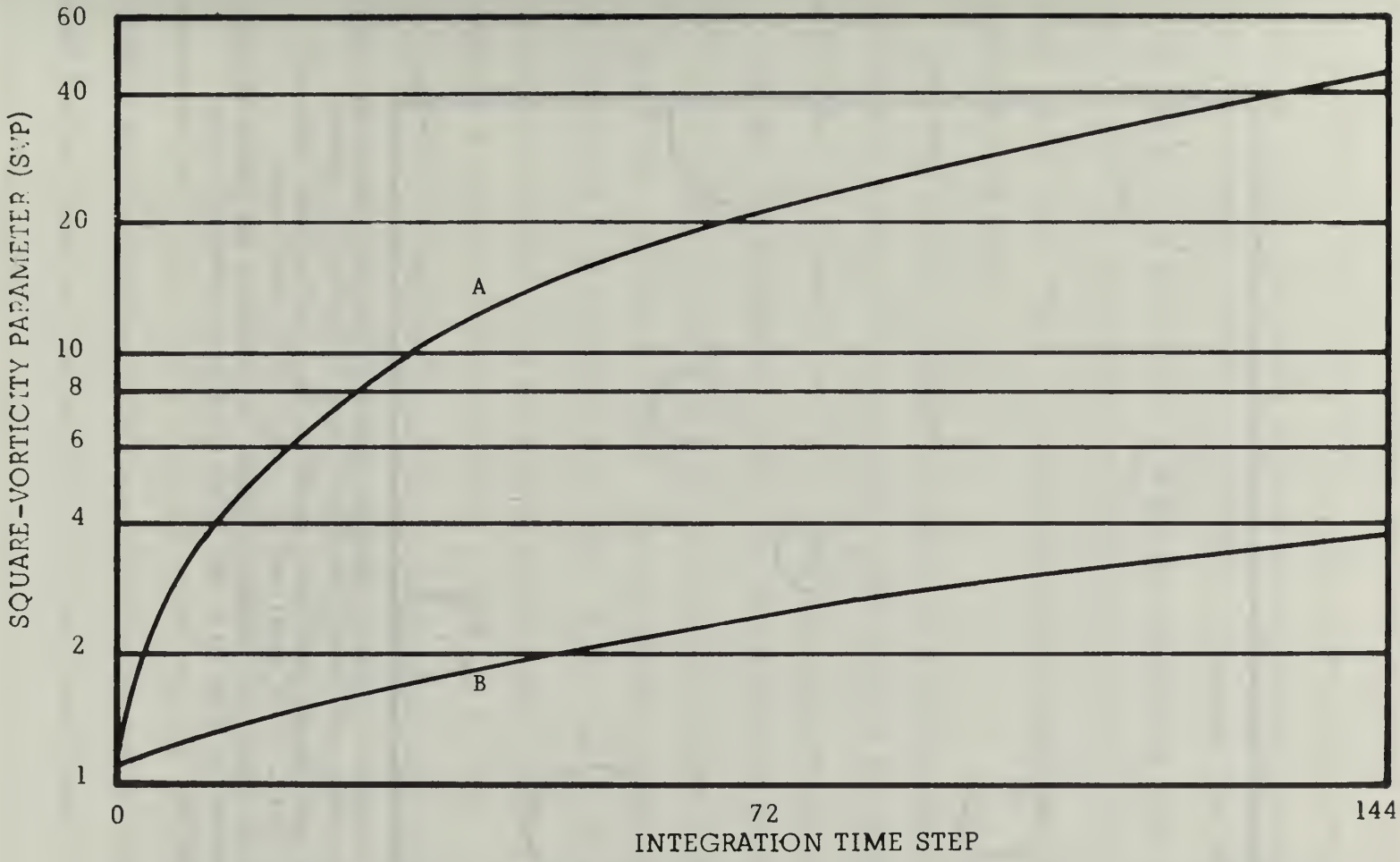

Figure 1. Square-Vorticity Parameter (SVP) as a function of time step. Curve A pertains to case with space averaging of terms. Curve B applies to cases in which no space averaging was employed; one in which the cycle was restarted after 36 steps; and one in which the cycle was never restarted. No significant SVP difference occurred in the latter cases.

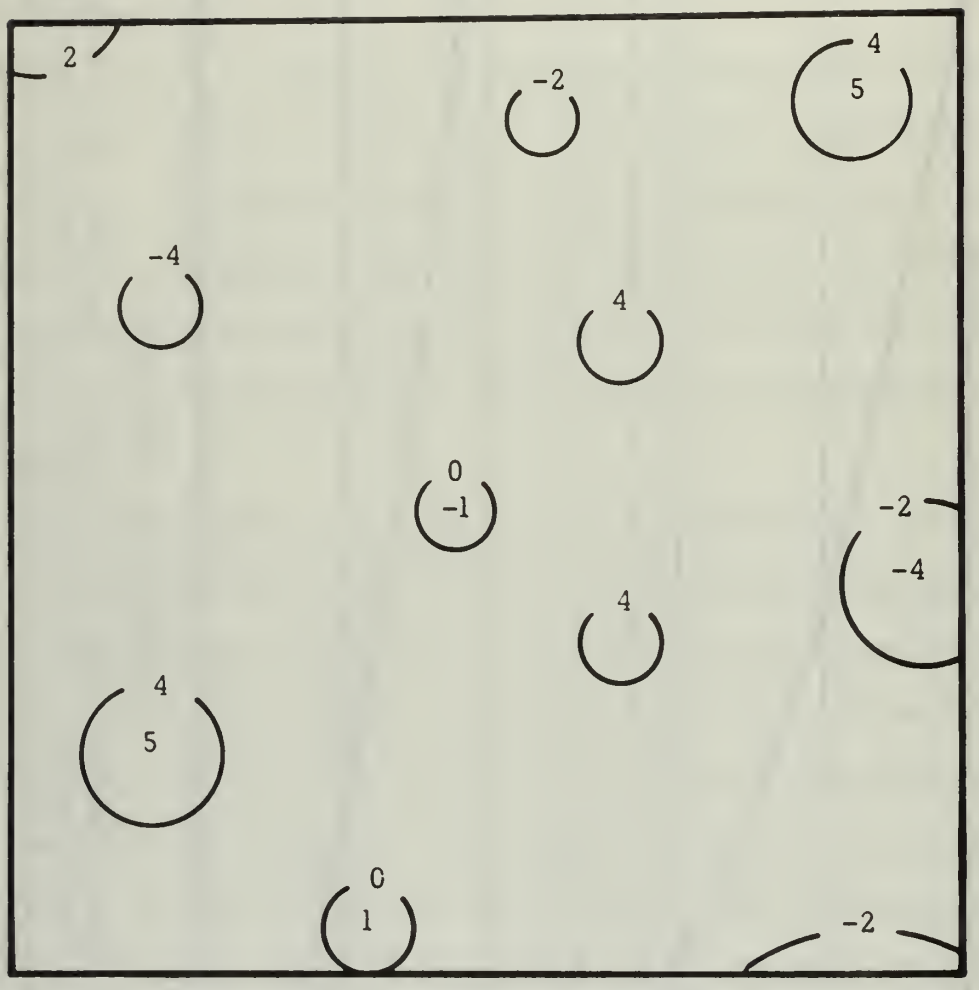

Figure 2. Difference Field (in meters) between the odd- and even-solution sets after 144 ten-minute time steps in barotropic experiment. This area shown represents a 10d x 10d subset of the total hemispheric field. It is idealized to portray the typical scale and magnitude of such a difference field. In general, the range of scale of features is from 2d to 4d, with magnitudes generally less than five meters.

A third test was made to measure the "departure" of the two solution sets. Figure 2 illustrates the (idealized) scale and magnitudes of the difference field after 144 time steps. Each side of the figure is ten mesh lengths long (about 3810 kilometers), and is representative of the entire hemispheric difference pattern. In general, the magnitudes of the centers are five meters or less after twenty-four hours of forecast period. This may be compared to the magnitude of the 500 MB diurnal height oscillation, which is (roughly) an order of magnitude larger than this difference field.

The mean kinetic energy was computed for each time step. No attempt was made to plot these distributions because the variation was negligible in the cases in which no space averaging was performed.

One test was attempted in which the latest odd- and even-step wind component and height fields were averaged (as appropriate) after 72 time steps, and then restarted. The calculations, however, blew up immediately after restarting the cycle. Thus, it would appear as though the "average" wind components and "average" heights introduce a considerable trauma in the system, in general. It should be noted that, at all other times, the restarting procedure involved using the latest fields rather than averaged fields.

Charts A through E depict the initial 500 MB analysis and daily forecast fields out to four days, respectively. The model tends to overdevelop both highs and lows, but it is felt that the phenomenon could be easily controlled. Note also that the amplitudes of small scale features increase perceptibly (with time), particularly in low latitudes. No attempt was made to control this accumulation of energy.

The barotropic primitive-equation 24-hour 500 MB forecast fields were compared with the barotropic filtered model output fields provided by FNWC. The height error fields revealed that the PE model output compared favorably with the operational FNWC model in the case tested. Charts F and G illustrate the height error patterns for the PE and filtered models, respectively, for the 24-hour period ending 0000Z, 25 April 1968. It was beyond the intent of this research to make more than a perfunctory comparison of these two models.

In summary, it can be said that the initialization through use of the linear balance equation was satisfactory when small-scale features were removed from the boundary regions by a latitudinally-varying filter. The boundary conditions and finite-difference forms used in the experiment were both economical and stable for integrations up to four days. Although the smaller-scale features tended to increase in amplitude, it was felt that the phenomenon could be easily controlled. The results would justify further research on a barotropic model initialized with real hemispheric data fields.

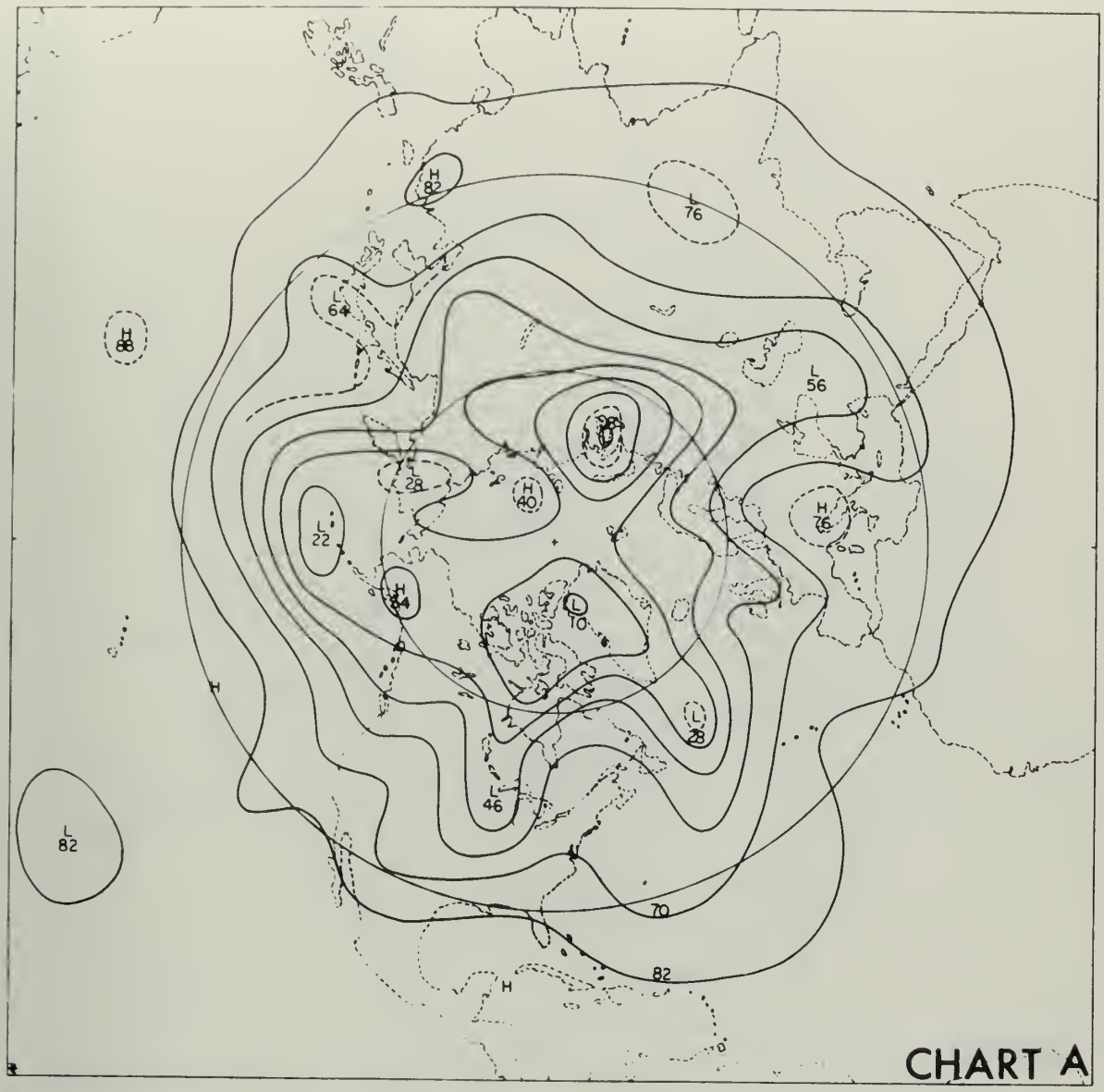

Chart A. Initial 500 MB Height Analysis for 0000Z, 24 April 1968.

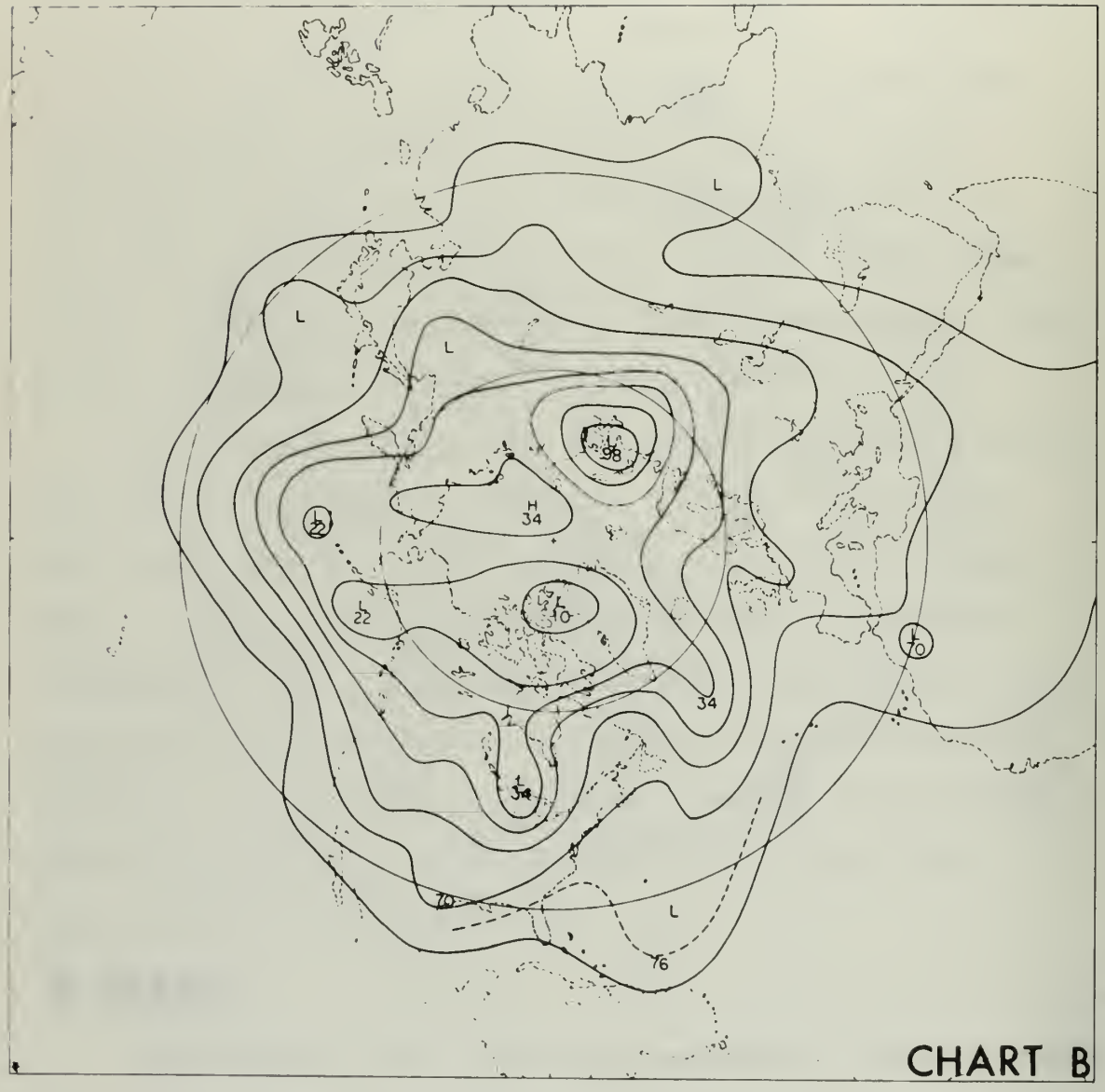

Chart B. P.E. Barotropic 500 MB 24-Hour Height Forecast from 0000Z, 24 April 1968.

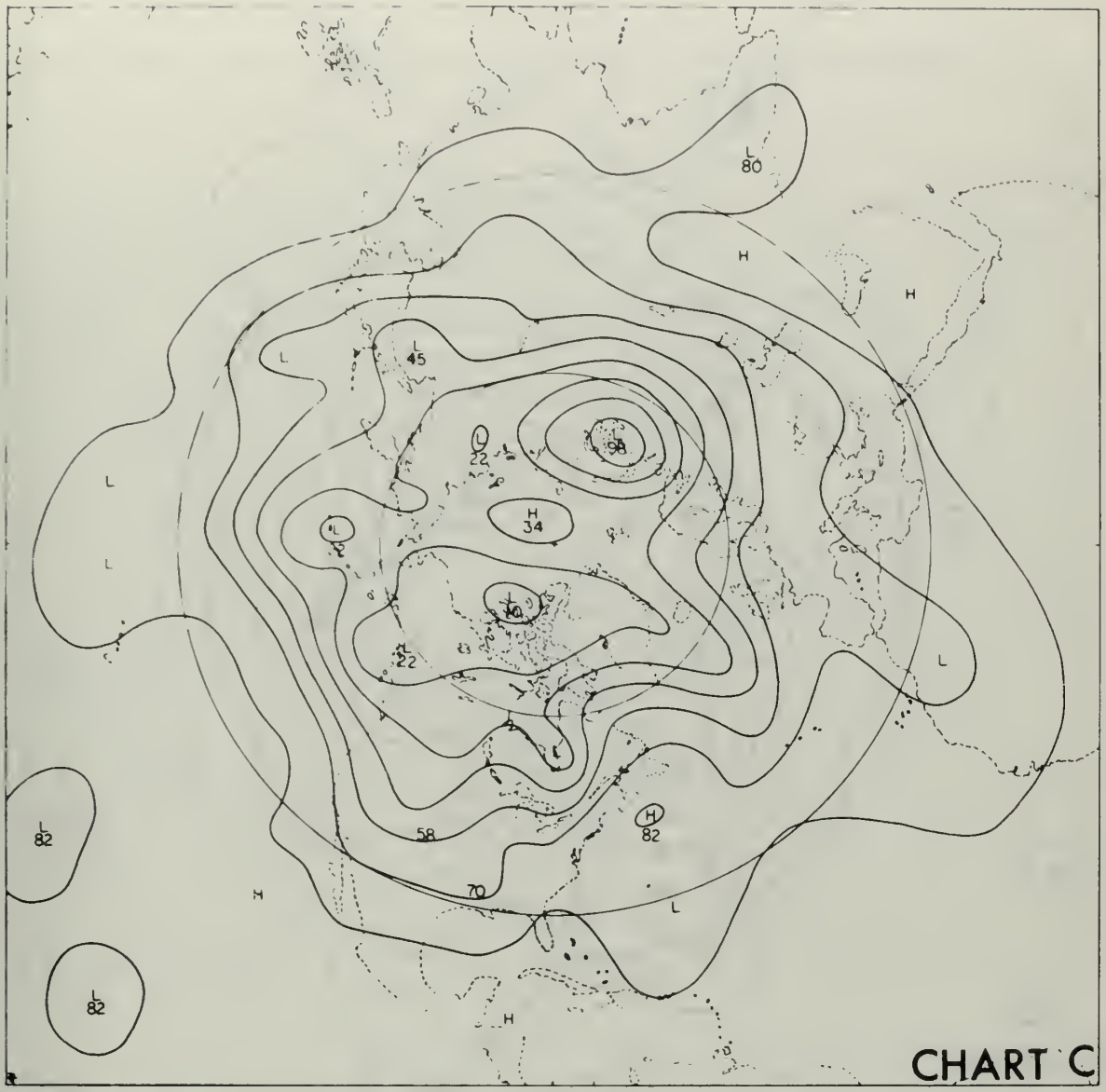

Chart C. P.E. Barotropic 500 MB 48-Hour Height Forecast from 0000Z, 24 April 1968.

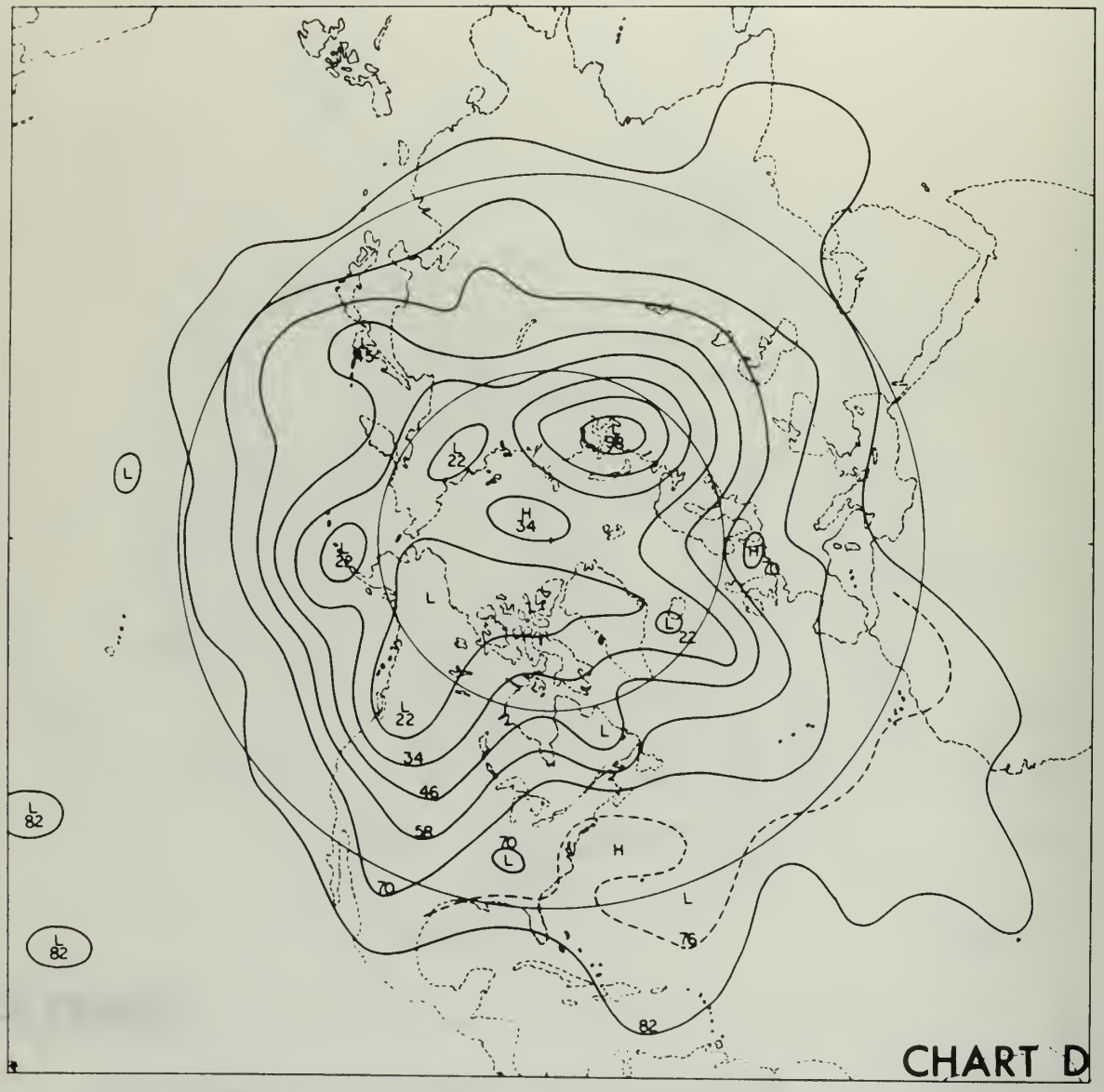

Chart D. P.E. Barotropic 500 MB 72-Hour Height Forecast from 0000Z, 24 April 1968.

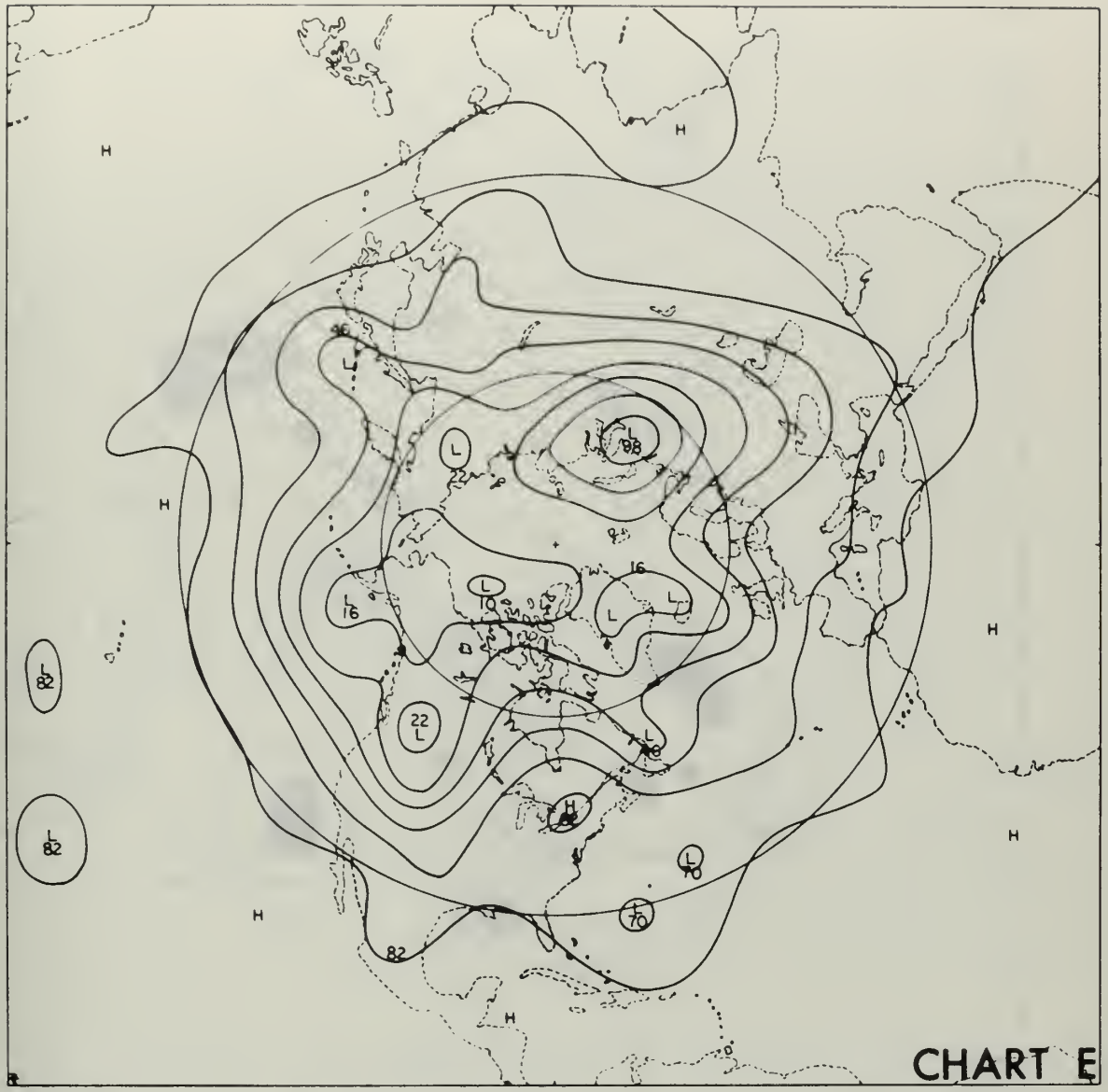

Chart E. P.E. Barotropic 500 MB 96-Hour Height Forecast from 0000Z, 24 April 1968.

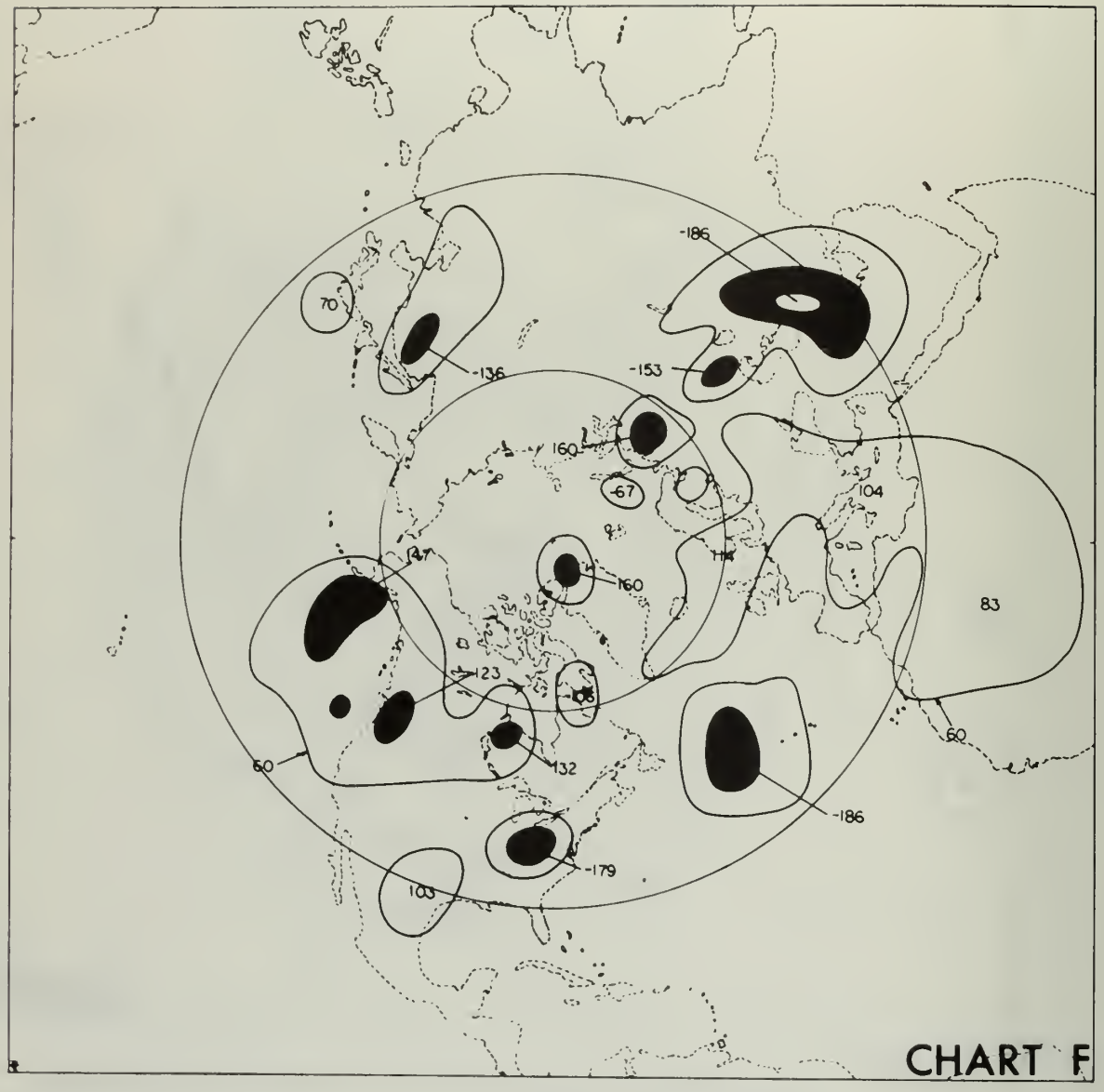

Chart F. P.E. Barotropic 24-Hour 500 MB Height Error Field (in meters) for period ending 0000Z, 25 April 1968.

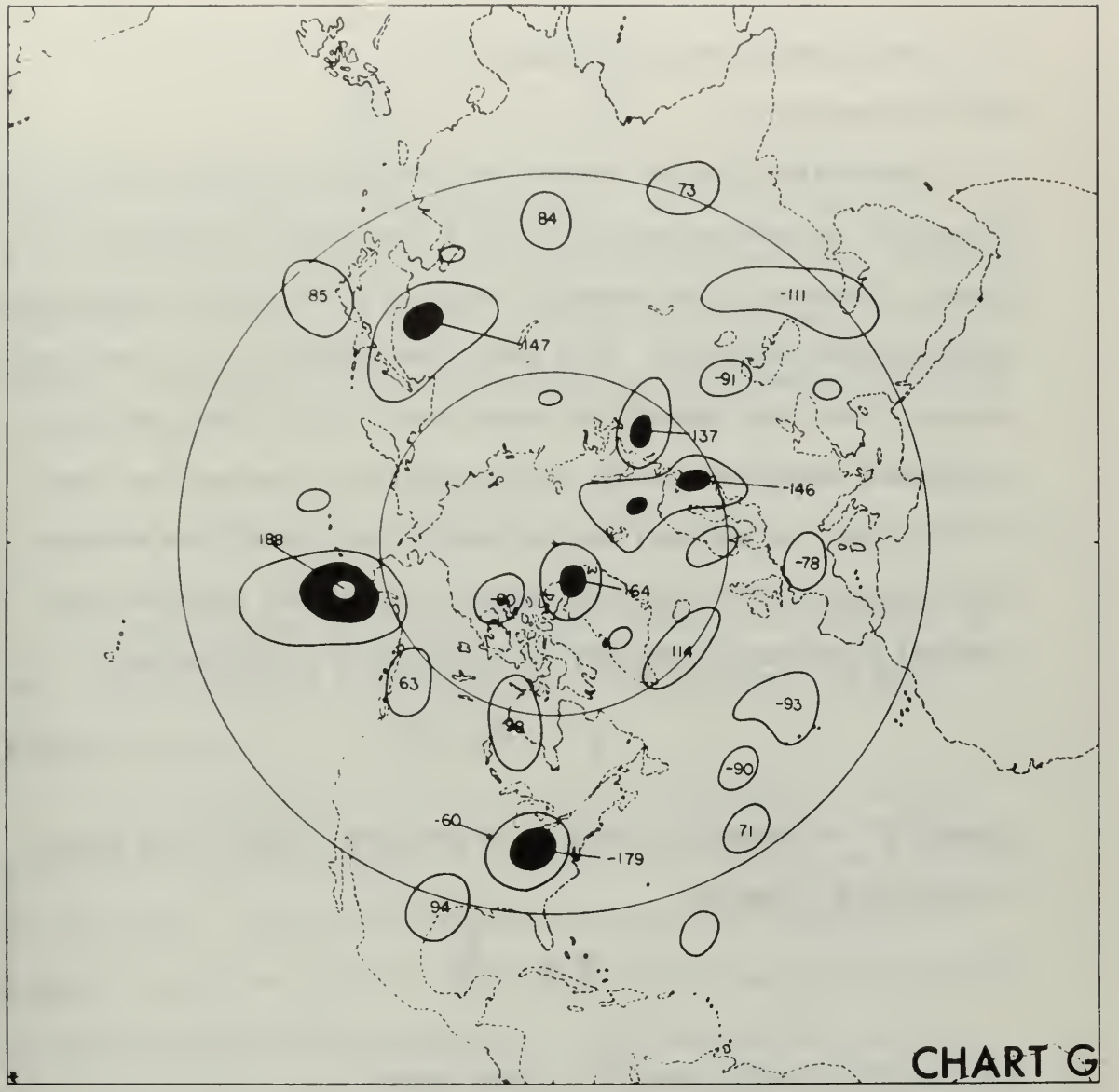

Chart G. FNWC (Vorticity Model) Barotropic 24-Hour 500 MB Error Field (in meters) for period ending 0000Z, 25 April 1968.

3.0 THE BAROCLINIC EXPERIMENT

3.1 Introduction

A generalized Fortran program was written for integrating an n-level baroclinic primitive-equation set for a frictionless, adiabatic atmosphere. Because of its generality, much of the possible computational economy was sacrificed. As a result, the frequent use of auxiliary memory (disc file) caused the expenditure of about twice as much peripheral processor time as central processor time per time step.

To check out and test run the model, the input-output section was written for five uniformly-spaced zeta (sigma) surfaces only. The vertical coordinate (zeta) may be given by the transformation

$$\sigma = f(\zeta) \tag{3.1.1}$$

where σ is defined as the ratio of pressure to that at the lower boundary (π); that is,

$$\sigma = \frac{p}{\pi} \tag{3.1.2}$$

Differentiation with respect to sigma leads to

$$\frac{\partial \zeta}{\partial \sigma} = \left(\frac{\partial f}{\partial \zeta}\right)^{-1} \tag{3.1.3}$$

which, in turn, suggested the definition of the so-called "vertical map factor"

$$S \equiv -\left(\frac{\partial f}{\partial \zeta}\right)^{-1} \tag{3.1.4}$$

This leads to the derivative transformation

$$\frac{\partial A}{\partial \sigma} = -s \frac{\partial A}{\partial z} \tag{3.1.5}$$

where A is an arbitrary dependent variable. In the special case used for evaluating the model, the transformation was linear and the vertical map factor, s, was equal to unity. Moreover, since zeta increased upward, the vertical velocity was defined positive upward according to the relation

$$w \equiv -\dot{\sigma} \tag{3.1.6}$$

It is well-known that Phillip's sigma system (and therefore, the zeta system) has both advantages and disadvantages. Its main advantages are:

a. the absence of one of the chief difficulties in pressure coordinates - that of needing to define the horizontal pressure gradient at sea level. For models that include terrain, the generation of ficticious pressure gradients is avoided because the terrain pressure is observed rather than calculated through some reduction scheme.

b. the function representing vertical motion vanishes identically at all material surfaces.

Two of the disadvantages of the sigma system are:

a. that observational data are generally taken at pressure surfaces. Thus, sigma surface parameters must be generated by some interpolation/extrapolation scheme.

b. that computational difficulties may arise because of large space variations of terrain pressure in certain regions (see Kurihara, 1968).

3.2 Purpose of the Baroclinic Experiment

Realizing that time would not permit the inclusion of diabatic heating and diffusion terms in the equations, the goal was made to program an n-level model for an adiabatic, inviscid atmosphere on a smooth earth; and to test the model at five uniformly-spaced zeta surfaces (in the time remaining). Provisions were made in the Fortran program to incorporate the remaining terms later without need for any major reprogramming effort.

As in the barotropic experiment, it remained to continue the evaluation of boundary conditions and initialization procedures. The modified-Arakawa conservation-type difference scheme had to be tested in the multi-level version. In addition, the author was aware of the buildup of energy in small-scale features in the barotropic model, and desired to observe the manifestations of frictionless flow in the more complex model.

3.3 The System of Prognostic Equations

The equation set for an inviscid, adiabatic atmosphere may be approximated on a polar stereographic map projection as follows:

a. east-west momentum equation:

$$\frac{\partial \pi u}{\partial t} = -m^2\left\{\frac{\partial}{\partial x}\left(\frac{\pi u^2}{m}\right)+\frac{\partial}{\partial y}\left(\frac{\pi uv}{m}\right)\right\} - \pi\dot{\sigma}\frac{\partial(\omega u)}{\partial \sigma}$$

$$+\pi v\left\{f-\frac{(vx-uy)}{2a^2}\right\} - m\left(\pi\frac{\partial \Phi}{\partial x}+RT\frac{\partial \pi}{\partial x}\right) \qquad (3.3.1)$$

b. north-south momentum equation:

$$\frac{\partial \pi v}{\partial t} = -m^2\left\{\frac{\partial}{\partial x}\left(\frac{\pi u v}{m}\right)+\frac{\partial}{\partial y}\left(\frac{\pi v^2}{m}\right)\right\} - \pi \dot{\sigma}\frac{\partial (w v)}{\partial \sigma}$$

$$-\pi u\left\{f-\frac{(vx-uy)}{2a^2}\right\}-m\left(\pi\frac{\partial \Phi}{\partial y}+RT\frac{\partial \pi}{\partial y}\right) \qquad (3.3.2)$$

c. continuity equation:

$$\frac{\partial \pi}{\partial t} = -m^2\left\{\frac{\partial}{\partial x}\left(\frac{\pi u}{m}\right)+\frac{\partial}{\partial y}\left(\frac{\pi v}{m}\right)\right\} - \pi \dot{\sigma}\frac{\partial w}{\partial \sigma} \qquad (3.3.3)$$

d. hydrostatic equation:

$$\frac{\partial \Phi}{\partial \sigma} = \frac{RT}{\sigma} \qquad (3.3.4)$$

e. thermodynamic equation:

$$\frac{\partial \pi T}{\partial t} = -m^2\left\{\frac{\partial}{\partial x}\left(\frac{\pi u T}{m}\right)+\frac{\partial}{\partial y}\left(\frac{\pi v T}{m}\right)\right\} - \pi \dot{\sigma}\frac{\partial (w T)}{\partial \sigma}$$

$$+\frac{RT}{\sigma c_p}\left[-\pi w+\sigma\left\{\frac{\partial \pi}{\partial t}+m\left(u\frac{\partial \pi}{\partial x}+v\frac{\partial \pi}{\partial y}\right)\right\}\right] \qquad (3.3.5)$$

where all symbols have been defined previously.

Figure 3 contains a diagram of computational levels with notations as to which variables are predicted or computed at those levels.

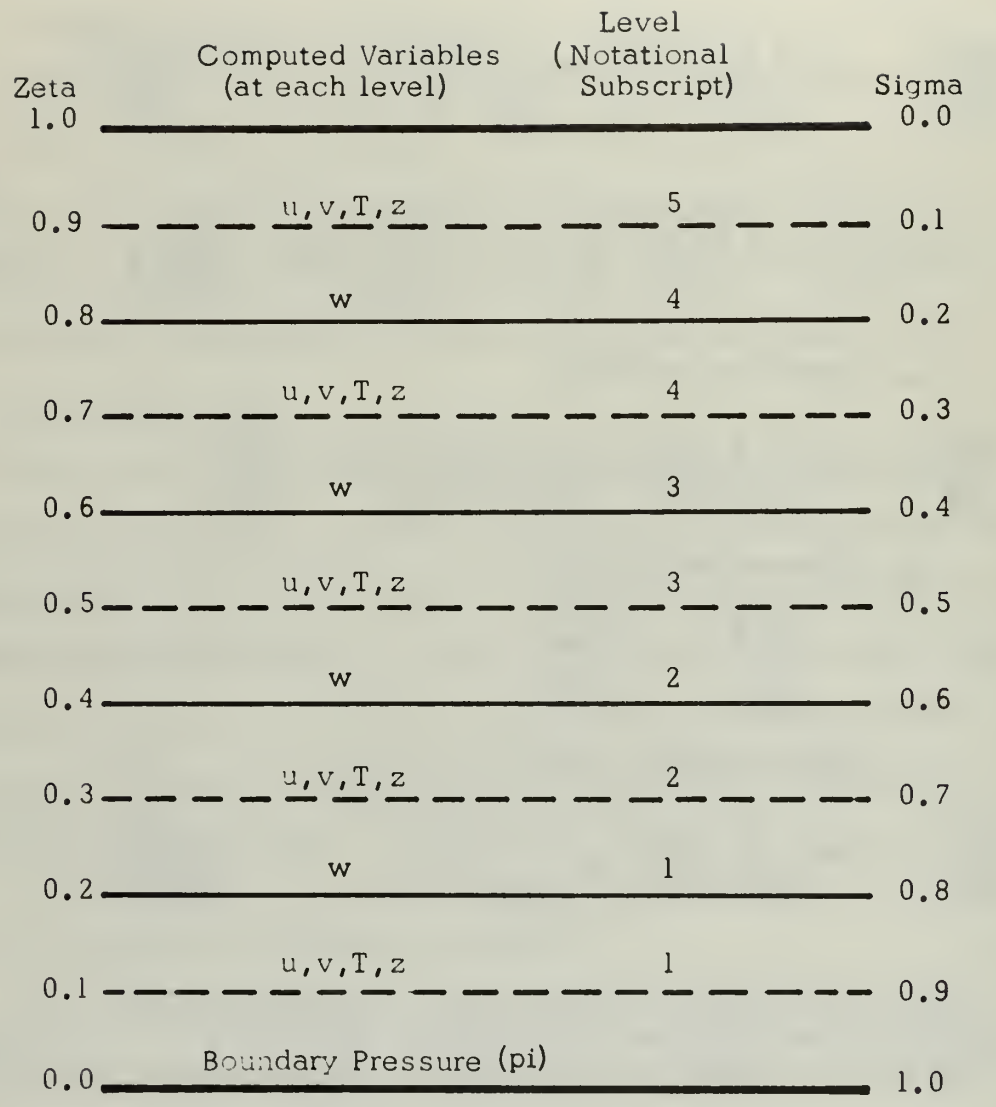

Figure 3. Diagram of Zeta (Sigma) Levels. Notations are made to indicate the subscripts used for the level, as well as to show the variables predicted or computed at each level. Note that "z" has been used interchangeably with phi (geopotential), and that "pi" has been used for the lower boundary pressure.

3.4 Finite-Difference Forms

The difference equations corresponding to (3.3) are based on the Arakawa technique. It will be noted that the set (3.3) are similar in form to those used earlier by Smagorinsky (1965).

The difference scheme avoids non-linear instability by requiring that the advective terms conserve the square of the advected property (when summed over the entire grid), assuming continuous time derivatives. The total energy is conserved because of requirements placed upon the vertical differencing; specifically, upon the special form of the hydrostatic equation. Assuming that the zeta surfaces are uniformly-spaced, the lowest phi distribution is given by

$$\bar{\Phi}_1 = \bar{\Phi}_{SFC} + \frac{R\Delta\sigma_1}{2}\left(\frac{T}{S\sigma}\right)_1 \qquad (3.4.1a)$$

and for subsequent levels, one uses

$$\bar{\Phi}_{K+1} = \bar{\Phi}_K + \frac{R\Delta\sigma_K}{2}\left\{\left(\frac{T}{S\sigma}\right)_{K+1} + \left(\frac{T}{S\sigma}\right)_K\right\} \qquad (3.4.1b)$$

It should be noted that a more complicated form of the hydrostatic equation is required if the surfaces are not uniformly-spaced. The reader is referred to Haltiner (3) for a complete discussion of the conservation properties of this difference scheme.

The east-west momentum equation is given by

$$(\pi u)_*^{m+1} = (\pi u)_*^{m-1} + 2\Delta t\left\{-\bar{f}(u)_* + \left[f_{i,j} - \frac{(VX-UY)_*}{2a^2}\right]\pi_{i,j}V_* - \frac{(m\pi)_{ij}}{2d}\left(\bar{\Phi}_{i+1,jk} - \bar{\Phi}_{i-1,jk}\right) - m_{ij}\frac{RT_*}{2d}\left(\pi_{i+1,j} - \pi_{i-1,j}\right)\right\}^m \qquad (3.4.2)$$

where (*) denotes the point (i,j,k).

Similarly, the north-south momentum equation is written

$$(\pi v)_*^{m+1} = (\pi v)_*^{m-1} + 2\Delta t \left\{ -f(v)_* - \left[f_{ij} - \left(\frac{vx - uy}{2a^2} \right)_* \right] \pi_{ij} u_* \right.$$

$$\left. - \frac{(m\pi)_{ij}}{2d} \left(\Phi_{i,j+1,k} - \Phi_{i,j-1,k} \right) - m_{ij} \frac{RT_*}{2d} \left(\pi_{i,j+1} - \pi_{i,j-1} \right) \right\}^m \qquad (3.4.3)$$

The lower boundary pressure is computed from

$$\pi_{ij}^{m+1} = \pi_{ij}^{m-1} + 2\Delta t \left(\frac{\partial \pi}{\partial t} \right)_{ij}^m \qquad (3.4.4)$$

where, for the entire column, one evaluates the local change as

$$\left(\frac{\partial \pi}{\partial t} \right)_{ij}^m = - \sum_{K=1}^{5} \frac{\Delta S_k m_{ij}^2}{2d} \left\{ \alpha_{i+1,jk} - \alpha_{i-1,jk} + \beta_{i,j+1,k} - \beta_{i,j-1,k} \right\}^m \qquad (3.4.5)$$

where, for notational convenience, one defines the quantities

$$\alpha = \frac{u\pi}{m}$$

and

$$\beta = \frac{v\pi}{m}$$

The thermodynamic equation takes on the form

$$(\pi T)_*^{m+1} = (\pi T)_*^{m-1} + 2\Delta t \left\{ -f(T)_* + \frac{RT_*}{\sigma_k c_p} \left[-\frac{\pi_{ij}}{2} \left(w_k + w_{k-1} \right)_{ij} \right. \right.$$

$$\left. \left. + \sigma_k \left(\frac{\partial \pi}{\partial t} \right)_{ij} + \sigma_k \frac{m_{ij}}{2d} \left[u_* \left(\pi_{i+1} - \pi_{i-1} \right)_j + v_* \left(\pi_{j+1} - \pi_{j-1} \right)_i \right] \right] \right\}^m \qquad (3.4.6)$$

Note that for any advected parameter an operator has been defined

$$\mathcal{L}(\psi)_* = \frac{m_{ij}^2}{4d}\left[\left\{(\alpha_{i+1}+\alpha_i)(\psi_{i+1}+\psi_i)-(\alpha_{i-1}+\alpha_i)(\psi_{i-1}+\psi_i)\right\}_{jk}\right.$$

$$\left.+\left\{(\beta_{j+1}+\beta_j)(\psi_{j+1}+\psi_j)-(\beta_{j-1}+\beta_j)(\psi_{j-1}+\psi_j)\right\}_{ik}\right]$$

$$+\frac{\pi_{ij}}{2}\left(\frac{s}{\Delta s}\right)_k\left[\omega_k(\psi_{k+1}+\psi_k)-\omega_{k-1}(\psi_k+\psi_{k-1})\right]_{ij} \qquad (3.4.7)$$

Finally, vertical motions for non-material surfaces are obtained from a form of the continuity equation

$$\omega_{ij,k+1} = \omega_* - \frac{\Delta s_k}{s_k \pi_{ij}}\left\{\left(\frac{\partial \pi}{\partial t}\right)_{ij} + \right.$$

$$\left.\frac{m_{ij}^2}{2d}\left[(\alpha_{i+1}-\alpha_{i-1})_{jk}+(\beta_{j+1}-\beta_{j-1})_{ik}\right]\right\} \qquad (3.4.8)$$

3.5 The Computational Sequence

For the initialization portion of the program, the sequence of steps is as follows:

a. compute map factor and Coriolis parameter.

b. read input fields from magnetic tape:

(1) sea level pressure.

(2) temperatures at 850, 700, 500, 400, 300, 200, and 100 MBS.

c. convert temperatures.

d. interpolate p-surface temperatures to build zeta-surface temperatures, and smooth fields in tropics.

e. form T-pi fields.

f. integrate hydrostatically to obtain phi fields.

g. solve linear balance equation at each level.

h. compute u- and v-components for each level.

i. form u-pi and v-pi fields.

For the steps involved in each time step after initialization is completed, the following are listed:

a. compute local change in lower boundary pressure.

b. compute vertical motion fields.

c. compute next lower boundary pressure.

d. compute forcing functions for momentum and thermodynamic equations for this level.

e. integrate to obtain next u-pi, v-pi, and T-pi fields for this level.

f. form next u, v, and T fields for this level.

g. repeat steps d. through f. for remaining levels.

h. compute next phi fields.

i. (optional) compute diagnostic parameters.

It should be noted that the integration cycle was restarted with a single forward time step every six hours in the baroclinic experiment.

3.6 Boundary Conditions

The boundary placement is identical to that used in the barotropic experiment. As in the barotropic experiment, the advective terms led to the following boundary conditions.

At the computational boundaries parallel to the y-axis,

$$\overline{\left(\frac{u\pi}{m}\right)}^{x} = 0 \tag{3.6.1a}$$

and

$$\frac{\partial \Phi}{\partial x} = \frac{\partial \pi}{\partial x} = 0 \tag{3.6.1b}$$

while, at the boundaries parallel to the x-axis,

$$\overline{\left(\frac{v\pi}{m}\right)}^{y} = 0 \tag{3.6.2a}$$

and

$$\frac{\partial \Phi}{\partial y} = \frac{\partial \pi}{\partial y} = 0 \tag{3.6.2b}$$

The practical imposition of boundary conditions was varied slightly from one test to another. For the most part, however, geostrophic flow was assumed at the first interior ring in order to avoid the necessity of estimating the values of "phi" and "pi" along the outermost ring. One-sided space derivitives were used in the continuity and thermodynamic equations (as appropriate) for computations along the first interior ring.

At the earth's surface and at the top of the atmosphere, the vertical velocity, w, vanished identically.

3.7 Initialization Procedures

The input fields for the baroclinic experiment were actual data fields as analyzed on the FNWC 63 x 63 hemispheric grid. To remove most of the disturbance components from the boundary regions, a latitudinally-dependent smoother of the form

$$S(\phi) = K_1(1-\sin\phi)^2 - K_2 \qquad (3.7.1)$$

was employed to compute the coefficient. The coefficient vanished north of 30° latitude.

Initialization of the geopotential and wind fields was accomplished by use of the linear balance equation for a sigma(zeta) surface. (It should be noted that the terms arising from the presence of the sphericity terms in the momentum equation were not retained.) The balance equation took on the form

$$\nabla^2\psi = \frac{1}{f}\left(\nabla^2\Phi + RT\left[\nabla^2\ln\pi - \left\{\left(\frac{\partial\ln\pi}{\partial x}\right)^2 + \left(\frac{\partial\ln\pi}{\partial y}\right)^2\right\}\right.\right.$$

$$\left.\left. + \frac{1}{T}\nabla T\cdot\nabla\ln\pi\right] - \nabla\psi\cdot\nabla f\right) \qquad (3.7.2)$$

as a result of the divergence of the two-termed pressure gradient force in sigma coordinates.

Appendix C contains a derivation of the divergence equation in sigma coordinates.

3.8 Research Procedures and Results

The generality of the Fortran program led to a very inefficient use of the CDC 6500 computer at the Fleet Numerical Weather Central. For the five-level version tested, approximately 180 disc accesses per time step were required (for storage of the history variables, and temporary storage of intermediate results). Because of the extremely heavy burden of high-priority operational programs being run on the FNWC computer in the period, October 1968 to December 1968, this phase of research was limited. In addition to "debugging" the 2000-instruction program, a few integrations were run out to twelve hours in order to make a few assessments of the output fields and measurements of the conservation parameters.

Interim results of the baroclinic experiment indicate the generation of static instabilities in the uppermost layers, and a subsequent rapid deterioration in the fields. No attempt was made to constrain the lapse rates of predicted temperatures.

The output fields at the sixth hour into the forecast did not show any indication of computational deterioration.

In almost every instance, the computational blow-up was accompanied by a catastrophic potential-to-kinetic energy conversion in the uppermost layers.

A continuing series of test runs are being made by the author in an effort to ascertain the source of the computational difficulties.

4.0 CONCLUSIONS AND RECOMMENDATIONS

4.1 The Barotropic Experiment

The barotropic experiment was intended to test the suitability of boundary conditions, initialization procedures, and the phrasing of the finite-difference analogs. In addition, some information as to the degree of smoothing of the initial data fields in the tropical regions was sought.

Initialization through use of the linear balance equation was satisfactory when most of the disturbance component was removed at the boundary region through use of a latitudinally-varying smoother routine.

The boundary conditions and finite-difference forms were found to be both economical and stable for integrations up to four days. (No runs were made beyond four days.)

Although energy tended to accumulate in the smaller ranges of scale, it was felt that this phenomenon could be controlled.

The results of this investigation would justify further research on a barotropic primitive-equation model that was initialized with real hemispheric data fields. The conservation properties of the difference scheme place the model at an advantage over the operational FNWC model for intermediate length integrations (three to seven days).

4.2 The Baroclinic Experiment

Since most of the test runs made indicated that instabilities developed in the first eight to thirteen hours of the forecast period, more work is required to ascertain the nature and cause(s) of the computational instabilities.

Preliminary results would seem to indicate that the vertical velocity fields were not satisfactory, generally. This was felt to be particularly true in the upper atmosphere, where sudden transformations of potential to kinetic energy were linked to unrealistic vertical transports, and the ensuing static instabilities.

The generalized Fortran program should be useful as a vehicle for future graduate research work at the Naval Postgraduate School. Provisions have been made for arbitrarily varying the number and location of zeta levels. In addition, heating and friction terms may be added without need for extensive reprogramming.

An extended core system (ECS) was added to the CDC 6500 computer in late December 1968, and will provided an additional 500,000 words of fast-access auxiliary memory. With little additional programming, this should greatly reduce the "field handling" time, and permit longer test runs.

BIBLIOGRAPHY

1. A. Arakawa, "Computational Design for Long-Term Numerical Integration of the Equations of Fluid Motion," Part I, JOURNAL OF COMPUTER PHYSICS, 1, 119-143, 1966.

2. G. Fischer, "A Survey of Finite-Difference Approximations to the Primitive Equations," MONTHLY WEATHER REVIEW, Volume 93, Number 1, January 1965.

3. G. Fischer, "On a Finite-Difference Scheme for Solving the Non-linear Primitive Equations for a Barotropic Fluid with application to the Boundary Current Problem," TELLUS, XVII (1965),4.

4. G.J. Haltiner, "Numerical Weather Prediction," Unpublished manuscript, 1968.

5. D. Houghton, A. Kasahara, and W. Washington, "Long-term Integration of the Barotropic Equations by the Lax-Wendroff Method," MONTHLY WEATHER REVIEW, Volume 94, Number 3, March 1966.

6. A. Kasahara, "On Certain Finite-Difference Methods for Fluid Dynamics," MONTHLY WEATHER REVIEW, Volume 93, Number 1, January 1965.

7. Y. Kurihara, "On the Use of Implicit and Iterative Methods for the Time Integration of the Wave Equation," MONTHLY WEATHER REVIEW, Volume 93, Number 1, January 1965.

8. Y. Kurihara, "Note on Finite-Difference Expressions for the Hydrostatic Relation and Pressure Gradient Force," MONTHLY WEATHER REVIEW, Volume 96, Number 9, September 1968.

9. D.K. Lilly, "On the Computational Stability of Numerical Solutions of Time_Dependent Non-linear Geophysical Fluid Dynamics Problems," MONTHLY WEATHER REVIEW, Volume 93, Number 1, January 1965.

10. K. Miyakoda and R.W. Moyer, "A Method of Initialization for Dynamical Weather Forecasting," TELLUS, XX (1968),1.

11. T. Nitta and J.B. Hovermale, "On Analysis and Initialization for the Primitive Forecast Equations," Weather Bureau Technical Memorandum NMC-42, October 1967.

12. N.A. Phillips, "A Coordinate System having some Special Advantages for Numerical Forecasting," JOURNAL OF METEOROLOGY, Volume 14, April 1957.

13. N.A. Phillips, "An Example of Non-linear Computational Instability," THE ATMOSPHERE AND SEA IN MOTION, 1959.

14. R.D. Richtmyer, "A Survey of Difference Methods for Non-Steady Fluid Dynamics," NCAR Technical Note 63-2, 1963.

15. F.G. Shuman, "Numerical Methods in Weather Prediction: I. The Balance Equation," MONTHLY WEATHER REVIEW, Volume 85, Number 10, October 1957.

16. F.G. Shuman, "Numerical Methods in Weather Prediction: II. Smoothing and Filtering," MONTHLY WEATHER REVIEW, Volume 85, Number 11, November 1957.

17. F.G. Shuman and L.W. Vanderman, "Difference System and Boundary Conditions for the Primitive-Equation Barotropic Forecast," MONTHLY WEATHER REVIEW, Volume 94, Number 5, May 1966.

18. F.G. Shuman and J.B. Hovermale, "An Operational Six-Layer Primitive-Equation Model," National Meteorological Center, October 1967.

19. J. Smagorinsky, S. Manabe, and J.L. Holloway, Jr., "Numerical Results from a Nine-Level General Circulation Model of the Atmosphere," MONTHLY WEATHER REVIEW, Volume 93, Number 12, December 1965.

20. J.A. Young, "Comparative Properties of Some Time Differencing Schemes for Linear and Non-linear Oscillations," MONTHLY WEATHER REVIEW, Volume 96, Number 6, June 1968.

APPENDIX A

Flux Forms of Barotropic Equations in Pressure Coordinates

The flux forms of the barotropic primitive-equation set in pressure coordinates may be "transformed" from the standard forms for a polar stereographic projection. These forms to be transformed are given by:

$$\frac{\partial u}{\partial t} = fv - m\left\{g\frac{\partial h}{\partial x} + \left(u\frac{\partial u}{\partial x} + v\frac{\partial u}{\partial y}\right)\right\} \tag{A.1a}$$

$$\frac{\partial v}{\partial t} = -fu - m\left\{g\frac{\partial h}{\partial y} + \left(u\frac{\partial v}{\partial x} + v\frac{\partial v}{\partial y}\right)\right\} \tag{A.1b}$$

$$\frac{\partial h}{\partial t} = -m\left\{h\left(\frac{\partial u}{\partial x} + \frac{\partial v}{\partial y}\right) + \left(u\frac{\partial h}{\partial x} + v\frac{\partial h}{\partial y}\right)\right\} \tag{A.2}$$

The procedure consists of showing that local change terms may be written as:

$$\frac{\partial u}{\partial t} = \frac{1}{h}\left\{\frac{\partial (uh)}{\partial t} - u\frac{\partial h}{\partial t}\right\} \tag{A.3a}$$

$$\frac{\partial v}{\partial t} = \frac{1}{h}\left\{\frac{\partial (vh)}{\partial t} - v\frac{\partial h}{\partial t}\right\} \tag{A.3b}$$

Similarly, the advective terms lead to the forms,

$$u\frac{\partial u}{\partial x} + v\frac{\partial u}{\partial y} = \frac{m}{h}\left[\left\{\frac{\partial}{\partial x}\left(\frac{hu^2}{m}\right) + \frac{\partial}{\partial y}\left(\frac{huv}{m}\right)\right\} + \frac{u}{m^2}\left\{\frac{\partial h}{\partial t} + h\left(u\frac{\partial m}{\partial x} + v\frac{\partial m}{\partial y}\right)\right\}\right] \tag{A.4a}$$

and

$$u\frac{\partial v}{\partial x}+v\frac{\partial v}{\partial y}=\frac{m}{h}\left[\left\{\frac{\partial}{\partial x}\left(\frac{huv}{m}\right)+\frac{\partial}{\partial y}\left(\frac{hv^2}{m}\right)\right\}\right.$$

$$\left.+\frac{v}{m^2}\left\{\frac{\partial h}{\partial t}+h\left(u\frac{\partial m}{\partial x}+v\frac{\partial m}{\partial y}\right)\right\}\right] \qquad \text{(A.4b)}$$

These terms may be substituted, as appropriate, in (A.1) to obtain:

$$\frac{\partial(uh)}{\partial t}=h\left\{+v-mg\frac{\partial h}{\partial x}-u\left(u\frac{\partial m}{\partial x}+v\frac{\partial m}{\partial y}\right)\right\}$$

$$-m^2\left\{\frac{\partial}{\partial x}\left(\frac{hu^2}{m}\right)+\frac{\partial}{\partial y}\left(\frac{huv}{m}\right)\right\} \qquad \text{(A.5a)}$$

$$\frac{\partial(vh)}{\partial t}=-h\left\{+u+mg\frac{\partial h}{\partial y}+v\left(u\frac{\partial m}{\partial x}+v\frac{\partial m}{\partial y}\right)\right\}$$

$$-m^2\left\{\frac{\partial}{\partial x}\left(\frac{huv}{m}\right)+\frac{\partial}{\partial y}\left(\frac{hv^2}{m}\right)\right\} \qquad \text{(A.5b)}$$

where the continuity equation is given by,

$$\frac{\partial h}{\partial t}=-m\left\{\frac{\partial}{\partial x}(uh)+\frac{\partial}{\partial y}(vh)\right\} \qquad \text{(A.6)}$$

It should be noted that (A.6) differs slightly from the usual flux form in which the map factor appears in both flux quantities. Thus, the initial divergence will not vanish identically (after use of the balance equation).

APPENDIX B

Energy Computations

In pressure coordinates the total potential energy (internal plus geopotential) may be written (for a smooth earth) as,

$$E_p = \frac{1}{g} \int_A \int_0^{p_o} c_p T \, dp \, dA \tag{B.1}$$

where "dA" represents an area increment. Now, if one eliminates $\delta\bar{\Phi}$ from the hydrostatic equations in pressure and zeta coordinates, respectively, one derives the relationship,

$$\delta\dot{p} = -\frac{P}{s\sigma}\delta\zeta = -\frac{\pi}{s}\delta\zeta \tag{B.2}$$

where "s" is the vertical mapping factor, and π is the lower boundary pressure (sea level). Substituting (B.2) in the first expression, the total potential energy becomes,

$$E_p = \frac{c_p}{g} \int_A \int_0^1 \frac{\pi T}{s} \, d\zeta \, dA \tag{B.3}$$

In a similar manner, the appropriate form for kinetic energy becomes,

$$E_K = \frac{1}{2g} \int_A \int_0^1 \frac{\pi}{s} (u^2 + v^2) \, d\zeta \, dA \tag{B.4}$$

The corresponding finite-difference forms for (B.3) and (B.4) were given as,

$$E_p = \frac{c_p D^2}{g} \sum_{\ell=1}^{L} \left(\frac{\Delta S}{S}\right)_\ell \sum_{i=1}^{N} \left(\frac{\Pi}{m^2}\right)_i T_{i,\ell} \qquad \text{(B.5)}$$

and

$$E_K = \frac{D^2}{2g} \sum_{\ell=1}^{L} \left(\frac{\Delta S}{S}\right)_\ell \sum_{i=1}^{N} \left(\frac{\Pi}{m^2}\right)_i \left(u^2 + v^2\right)_{i,\ell} \qquad \text{(B.6)}$$

where "N" is the number of mesh areas and "L" is the number of layers. In addition, "D" is the grid mesh length, and other symbols were as initially specified.

APPENDIX C

Divergence Equation Forms in the Sigma System

One can take the divergence of the vector equation of frictionless, adiabatic motion on a sigma surface and show that the resulting divergence equation assumes the form,

$$\frac{d\hat{\delta}}{dt} + \hat{\delta}^2 - f\hat{\zeta}_\sigma - 2J(u,v) + \nabla\dot{\sigma}\cdot\frac{\partial \mathbf{V}}{\partial\sigma} + \nabla^2\Phi - u\frac{\partial f}{\partial x}$$

$$+ v\frac{\partial f}{\partial y} + RT\left[\nabla^2 \ln\pi - \left\{\left(\frac{\partial \ln\pi}{\partial x}\right)^2 + \left(\frac{\partial \ln\pi}{\partial y}\right)^2\right\} + \frac{1}{T}\nabla T\cdot\nabla\ln\pi\right] = 0 \quad \text{(C.1)}$$

if the "sphericity" terms are omitted from the equation of motion.

It has been shown (see Haltiner (3), for example) that the terms of significance to less-generalized vorticity models specialize to

$$\nabla^2\psi = \frac{1}{f}\left\{\nabla^2\Phi - \nabla\psi\cdot\nabla f\right\} \quad \text{(C.2)}$$

usually referred to as the linear balance equation, under the assumption that the non-divergent component of the wind is large compared to the divergent component.

In sigma coordinates, however, terms arising from the additional pressure force term in the momentum equations are rather large, and must be included in the balance equation in sigma coordinates. The resulting form is given as

$$\nabla^2\Phi - f\nabla^2\psi - \nabla\psi\cdot\nabla f + RT\left[\nabla^2\ln\pi + \frac{1}{T}\nabla T\cdot\nabla\ln\pi\right.$$

$$\left. - \left\{\left(\frac{\partial \ln\pi}{\partial x}\right)^2 + \left(\frac{\partial \ln\pi}{\partial y}\right)^2\right\}\right] = 0 \quad \text{(C.3)}$$

If one applies the $(\hat{k}\cdot\nabla\times\ )$ operator to the same equation of motion, the vertical component of the relative vorticity on a sigma surface is found to be

$$\hat{\zeta}_\sigma = \frac{1}{f}\left[\nabla^2\Phi + RT\left\{\nabla^2\ln\pi - \left[\left(\frac{\partial\ln\pi}{\partial x}\right)^2 + \left(\frac{\partial\ln\pi}{\partial y}\right)^2\right] + \frac{1}{T}\nabla T\cdot\nabla\ln\pi\right\}\right] \quad (C.4)$$

which preserves the mathematical form of the linear balance equation. It should be noted that (C.3) takes on a more complicated form when the term

$$\mp \frac{(vX - uY)}{2a^2}(u,v)^*\pi$$

is added to the momentum equations.

* as appropriate

THESIS DISTRIBUTION LIST

		Copies
1.	LT Philip G. Kesel, USN Fleet Numerical Weather Central NPGS, Monterey, California 93940	5
2.	Professor G.J. Haltiner Department of Meteorology NPGS, Monterey, California 93940	3
3.	Professor R.T. Williams Department of Meteorology NPGS, Monterey, California 93940	3
4.	Library, Naval Postgraduate School Monterey, California 93940	2
5.	Defense Documentation Center Cameron Station Alexandria, Virginia 22314	20
6.	Naval Weather Service Command Washington Navy Yard Wasington, D.C. 20390	1
7.	Officer in Charge, NWRF Naval Air Station, Bldg. R-48 Norfolk, Virginia 23511	1
8.	Commanding Officer FNWC, NPGS Monterey, California 93940	2
9.	AFCRL - Research Library L.G. Hanscom Field (Attn: Nancy Davis, Stop 29) Bedford, Massachusetts 01730	1
10.	Dr. G.B. Tucker Commonwealth Bureau of Meteorology P.O. Box 1289 K Melbourne, Vic, Australia	1
11.	Department of Meteorology (Code 51) Naval Postgraduate School Monterey, California 93940	3

12.	Department of Oceanography (Code 58) Naval Postgraduate School Monterey, California 93940	1
13.	American Meteorological Society 45 Beacon Street Boston, Massachusetts 02128	1
14.	Commander, Air Weather Service (MAC) U.S. Air Force Scott AFB, Illinois 62226	2
15.	Atmospheric Sciences Library Environmental Science Service Administration Silver Spring, Maryland 20910	1
16.	Oceanographer of the Navy The Madison Building 732 N. Washington Street Alexandria, Virginia 22314	1
17.	Naval Oceanographic Office Attn: Library Washington, D.C. 20390	1
18.	Naval Oceanographic Data Center Washington, D.C. 20390	1
19.	Director, Maury Center for Ocean Sciences Naval Research Laboratory Washington, D.C. 20390	1
20.	Dr. A. Arakawa UCLA Department of Meteorology Los Angeles, California 90024	1
21.	Professor N.A. Phillips MIT 54-1422 Cambridge, Massachusetts 02139	1
22.	Dr. F.H. Bushby Meteorology Office Bracknell, England	1
23.	Dr. F.G. Shuman Director, NMC, ESSA Suitland, Maryland	1

DOCUMENT CONTROL DATA - R&D
(Security classification of title, body of abstract and indexing annotation must be entered when the overall report is classified)

1. ORIGINATING ACTIVITY (Corporate author)
Naval Postgraduate School
Monterey, California 93940

2a. REPORT SECURITY CLASSIFICATION
Unclassified

2b. GROUP

3 REPORT TITLE
EXPERIMENTS WITH ATMOSPHERIC PRIMITIVE-EQUATION MODELS

4. DESCRIPTIVE NOTES (Type of report and inclusive dates)
Master's Thesis, 1968

5. AUTHOR(S) (Last name, first name, initial)
KESEL, Philip G., LT, USN

6. REPORT DATE	7a. TOTAL NO. OF PAGES	7b. NO. OF REFS
December 1968	60	20

8a CONTRACT OR GRANT NO.	9a. ORIGINATOR'S REPORT NUMBER(S)
b. PROJECT NO.	
c.	9b. OTHER REPORT NO(S) (Any other numbers that may be assigned this report)
d.	

10. AVAILABILITY/LIMITATION NOTICES
Distribution of this document is unlimited.

11. SUPPLEMENTARY NOTES	12. SPONSORING MILITARY ACTIVITY
	Naval Postgraduate School Monterey, California 93940

13 ABSTRACT

Two atmospheric prediction models, based upon the meteorological primitive equations, were programmed and tested on the CDC 6500 computer. A frictionless, barotropic model was integrated, using ten-minute time steps, at 500 MBS for periods up to four days. Then, an n-level, baroclinic model for an inviscid, adiabatic atmosphere was integrated for brief test periods at five uniformly-spaced zeta (sigma) surfaces over a smooth earth. Both models were initialized with actual data fields provided by FNWC Monterey.

Acceptability was based on measurements of energy and vorticity parameters, as well as on qualitative assessments of output fields. The barotropic 500 MB height forecasts were found to be comparable to the FNWC (vorticity model) barotropic forecasts. Mean-square-vorticity and kinetic energy were suitably conserved for integrations up to four days. An energy accumulation in the smaller range of scale was increasingly evident beyond two days into the forecast period. No smoothing was performed to control this accumulation. A limited number of test integrations was made with the five-level model. Computational instabilities were observed for forecasts beyond twelve hours. Interim results are presented.

DD FORM 1 JAN 64 1473

14 KEY WORDS	LINK A		LINK B		LINK C	
	ROLE	WT	ROLE	WT	ROLE	WT
PRIMITIVE-EQUATION MODELS BAROTROPIC P.E. MODELS BAROCLINIC P.E. MODELS INTEGRATION OF ATMOSPHERIC PRIMITIVE-EQUATIONS